Momentum Transfer Dynamics of a Gyrostat With a Discrete Damper[1]

Christopher D. Hall[2]

Aerospace and Ocean Engineering,

Virginia Polytechnic Institute and State University,

Blacksburg, Virginia 24061-0203

Abstract

The stability of motion of attitude maneuvers of a torque-free rigid gyrostat with a discrete damper is investigated. The equations of motion are presented and non-dimensionalized, then rewritten as a singularly perturbed, noncanonical, Hamiltonian system. Conditions for equilibrium motions and for their stability are developed. Bifurcation diagrams are used to illustrate the stable and unstable branches of steady spins, and these bifurcation diagrams are interpreted in the slow state space of the rotor momenta and the unperturbed system Hamiltonian. Numerical integration is used to compute representative momentum transfer trajectories, which are also interpreted as projections onto the slow state space. We are especially interested in identifying regions of phase space through which momentum transfer maneuvers might reasonably be expected to succeed, but which are destabilized by the presence of the damping mechanism.

Introduction

Asymptotic stability of steady spins of satellites depends on the effective use of energy dissipation to damp out coning motions caused by perturbing torques. It is also important to consider the effects of energy dissipation on the stability of motion during large-angle rotational maneuvers. A thorough investigation of the stability of steady spins of rigid bodies and of rigid gyrostats including "energy sinks" and discrete dampers is presented by Hughes.[1] A recent paper by Chang *et*

[1]Presented as Paper 97-0107 at the 35th Aerospace Sciences Meeting, Reno, NV, January 6-10, 1997.

[2]Assistant Professor of Aerospace Engineering. Associate Fellow AIAA.

al.[2] gives an excellent overview of the types of damper mechanisms used in spacecraft, with references to papers on the various types. In an earlier paper,[3] we obtained some new results on the bifurcations in stability that occur for a rigid body with a discrete damper situated in a principal plane and aligned parallel to the nominal spin axis (the major axis). The purpose of the present paper is to present the results of applying similar analyses to the motion of a rigid body containing several flywheels that are used to absorb perturbing torques (*i.e.*, reaction wheels) or to reorient the platform (*i.e.*, momentum wheels). The study of the rotational maneuvers of spacecraft with a single rotor has received much attention in the literature, with important results given in Refs. 4–7 and 8. The effects of a torsionally flexible appendage were included in Ref. 9. For multiple rotors, there are fewer results, but some work has been published in Refs. 6, 10, and 11. In this paper, the momentum transfer analyses developed in Refs. 12, 13, and 14 are extended to include the effects of the discrete damper.

Model and Equations of Motion

The model we study is shown in Fig. 1, consisting of a rigid body, $\mathcal{B}$, containing N rigid axisymmetric rotors, $\mathcal{R}_j$, and a mass particle $\mathcal{P}$, which is constrained to move along a line $\vec{\mathbf{n}}$ fixed in $\mathcal{B}$. The particle is connected to a linear spring and a liner dashpot damper. The reference axes $\vec{\mathbf{b}}_i$ are fixed in the body, but are not necessarily the system principal axes when $\mathcal{P}$ is in its rest position $(x^* = 0)$. All vectors and tensors are expressed with respect to the body frame. This is a reasonable model for a spacecraft with momentum wheels and a "ball-in-tube" type damper. It is also a reasonable model for approximating the motion of a spacecraft with a flexible appendage when only the first vibrational mode of the appendage is of interest. In the former case the mass of the particle would typically be a small fraction of the total mass, whereas in the latter case, the mass fraction may be more significant.

The dimensional equations of motion are developed following Hughes,[1] and nondimensionalized as in Chinnery and Hall.[3] The system linear and angular momentum are denoted by $\mathbf{p}^*$ and

$\mathbf{h}^*$, respectively. (The superscript $*$ is used to denote dimensional quantities; we nondimensionalize the equations below.) The linear momentum of the particle in the $\mathbf{n}$ direction is p_n^*, and the relative position and velocity of the particle in the $\mathbf{n}$ direction are x^* and y^*. The angular velocity of the body frame is $\boldsymbol{\omega}^*$, and the velocity of the point $\mathbf{O}$ is $\mathbf{v}_o^*$. The j_{th} rotor, $\mathcal{R}_j$, has axial angular momentum $h_{sj}^* = I_{sj}^* \omega_{sj}^*$ relative to the platform, and is subject to an axial torque g_{aj}^* applied by the platform. Collectively, these are denoted $\mathbf{h}_s^*$ and $\mathbf{g}_a^*$. The position vector from $\mathbf{O}$ to $\mathcal{P}$ is $\mathbf{r}_p^* = \mathbf{b}^* + x^* \mathbf{n}$, where $\mathbf{b}^*$ is a vector from the point $\mathbf{O}$ to the undeformed position of the particle, $\mathbf{n}$ is a unit vector in the direction of travel of the particle, and x^* is the deflection of the particle. The mass of the particle is m_p^*, and the total mass is m^*. The first and second moments of inertia with respect to $\mathbf{O}$ are $\mathbf{c}^*$ and $\mathbf{I}^*$. The moment of inertia matrix depends on the location of the mass particle. The symbol $\mathbf{I}_o^*$ denotes the moment of inertia when the particle is in its nominal position ($x^* = 0$). The spring has stiffness k^*, and the dashpot damper has damping coefficient c_d^*.

Dimensional Equations of Motion

In terms of these variables and parameters, the equations describing torque- and force-free motion are:

$$\mathbf{p}^* = m^* \mathbf{v}_o^* \Leftrightarrow \mathbf{c}^{*\times} \boldsymbol{\omega}^* + m_p^* y^* \mathbf{n} \tag{1}$$

$$\mathbf{h}^* = \mathbf{c}^{*\times} \mathbf{v}_o^* + \mathbf{I}^* \boldsymbol{\omega}^* + \mathbf{A} \mathbf{I}_s^* \boldsymbol{\omega}_s^* + m_p^* y^* \mathbf{b}^{*\times} \mathbf{n} \tag{2}$$

$$\mathbf{h}_a^* = \mathbf{I}_s^* (\mathbf{A}^T \boldsymbol{\omega}^* + \boldsymbol{\omega}_s^*) \tag{3}$$

$$p_n^* = m_p^* (\mathbf{n}^T \mathbf{v}_o^* \Leftrightarrow \mathbf{n}^T \mathbf{b}^{*\times} \boldsymbol{\omega}^* + y^*) \tag{4}$$

$$\dot{\mathbf{p}}^* = \Leftrightarrow \boldsymbol{\omega}^{*\times} \mathbf{p}^* \tag{5}$$

$$\dot{\mathbf{h}}^* = \Leftrightarrow \boldsymbol{\omega}^{*\times} \mathbf{h}^* \Leftrightarrow \mathbf{v}_o^{*\times} \mathbf{p}^* \tag{6}$$

$$\dot{\mathbf{h}}_a^* = \mathbf{g}_a^* \tag{7}$$

$$\dot{p}_n^* = m_p^* \boldsymbol{\omega}^{*T} \mathbf{n}^\times (\mathbf{v}_o^* \Leftrightarrow \mathbf{r}_p^{*\times} \boldsymbol{\omega}^*) \tag{8}$$

$$\Leftrightarrow c_d^* y^* \Leftrightarrow k^* x^*$$

$$\dot{x}^* = y^* \tag{9}$$

The superscript $\times$ denotes the skew-symmetric matrix form of a vector.[1]

Dimensionless Equations of Motion

To nondimensionalize, we scale the variables and parameters as follows:

$$\begin{aligned}
\mathbf{p}^* &= (h^* m^* b^*/I_c^*)\mathbf{p} & \mathbf{h}^* &= h^* \mathbf{h} \\
p_n^* &= (h^* m^* b^*/I_c^*)p_n & \mathbf{v}_o^* &= (h^* b^*/I_c^*)\mathbf{v}_o \\
\boldsymbol{\omega}^* &= (h^*/I_c^*)\boldsymbol{\omega} & y^* &= (h^* b^*/I_c^*)y \\
x^* &= b^* x & \boldsymbol{\omega}_s^* &= (h^*/I_c^*)\boldsymbol{\omega}_x \\
t^* &= (I_c^*/h^*)t & \mathbf{h}_a^* &= h^* \mathbf{h}_a \\
\mathbf{b}^* &= b^* \mathbf{b} & \mathbf{c}^* &= m_p^* x^* \mathbf{n} \\
\mathbf{I}^* &= I_c^* \mathbf{I} & \mathbf{I}_s^* &= I_c^* \mathbf{I}_s \\
\varepsilon &= m_p^*/m^* & b &= m^* b^{*2}/I_c^* \\
c_d &= c_d^* I_c^*/(m^* h^*) & k &= k^* I_c^{*2}/(m^* h^{*2})
\end{aligned} \tag{10}$$

where $h^* = ||\mathbf{h}^*||$ is the constant magnitude of the angular momentum vector. The dimensionless equations of motion are then

$$\mathbf{p} = \mathbf{v}_o \Leftrightarrow \varepsilon x \mathbf{n}^\times \boldsymbol{\omega} + \varepsilon y \mathbf{n} \tag{11}$$

$$\mathbf{h} = \varepsilon b x \mathbf{n}^\times \mathbf{v}_o + \mathbf{I}\boldsymbol{\omega} + \mathbf{A}\mathbf{I}_s \boldsymbol{\omega}_s + \varepsilon b y \mathbf{b}^\times \mathbf{n} \tag{12}$$

$$\mathbf{h}_a = \mathbf{I}_s(\mathbf{A}^T \boldsymbol{\omega} + \boldsymbol{\omega}_s) \tag{13}$$

$$
\begin{aligned}
p_n &= \varepsilon(\mathbf{n}^T\mathbf{v}_o \Leftrightarrow \mathbf{n}^T\mathbf{b}^\times\boldsymbol{\omega} + y) && (14)\\
\dot{\mathbf{p}} &= \Leftrightarrow\boldsymbol{\omega}^\times\mathbf{p} && (15)\\
\dot{\mathbf{h}} &= \Leftrightarrow\boldsymbol{\omega}^\times\mathbf{h} \Leftrightarrow b\mathbf{v}_o^\times\mathbf{p} && (16)\\
\dot{\mathbf{h}}_a &= \mathbf{g}_a && (17)\\
\dot{p}_n &= \varepsilon\boldsymbol{\omega}^T\mathbf{n}^\times[\mathbf{v}_o \Leftrightarrow (\mathbf{b} + x\mathbf{n})^\times\boldsymbol{\omega}] && (18)\\
&\quad \Leftrightarrow c_d y \Leftrightarrow kx\\
\dot{x} &= y && (19)
\end{aligned}
$$

The dimensionless moment of inertia matrix is

$$
\begin{aligned}
\mathbf{I} = \mathbf{I}_o + \varepsilon b\Big[\left(2x\mathbf{b}^T\mathbf{n} + x^2\right)\mathbf{1}\Leftrightarrow \\
x(\mathbf{b}\mathbf{n}^T + \mathbf{n}\mathbf{b}^T) \Leftrightarrow x^2\mathbf{n}\mathbf{n}^T\Big]
\end{aligned} \qquad (20)
$$

Reduced Order Equations of Motion

Under the assumption of zero external force and moment, we can eliminate the linear momentum and the velocities, reducing the equations to a system of $5 + N$ equations for $\mathbf{h}$, $\mathbf{h}_a$, p_n, and x:

$$
\begin{aligned}
\dot{\mathbf{h}} &= \mathbf{h}^\times\mathbf{J}^{-1}\mathbf{m} && (21)\\
\dot{\mathbf{h}_a} &= \mathbf{g}_a && (22)\\
\varepsilon\dot{p}_n &= \Leftrightarrow c_d y \Leftrightarrow \varepsilon kx && (23)\\
&\quad \Leftrightarrow \varepsilon^2\mathbf{m}^T\mathbf{J}^{-1}\mathbf{n}^\times[(\varepsilon' x\mathbf{n} + \mathbf{b})^\times\mathbf{J}^{-1}\mathbf{m}]\\
\varepsilon\dot{x} &= \varepsilon y && (24)
\end{aligned}
$$

where $\varepsilon' = 1 \Leftrightarrow \varepsilon$, and

$$\begin{aligned} \mathbf{J} &= \mathbf{I}_o \Leftrightarrow \mathbf{A}\mathbf{I}_s\mathbf{A}^T \Leftrightarrow \varepsilon\varepsilon' b x^2 \mathbf{n}^\times \mathbf{n}^\times \\ &\quad + \varepsilon b \left[2x\mathbf{b}^T\mathbf{n}\mathbf{1} \Leftrightarrow x(\mathbf{b}\mathbf{n}^T + \mathbf{n}\mathbf{b}^T) \right] \end{aligned} \tag{25}$$

$$\mathbf{m} = \mathbf{h} \Leftrightarrow \mathbf{A}\mathbf{h}_a \Leftrightarrow \varepsilon b y \mathbf{b}^\times \mathbf{n} \tag{26}$$

$$\varepsilon y = \frac{p_n + \varepsilon \mathbf{n}^T \mathbf{b}^\times \mathbf{J}^{-1}(\mathbf{h} \Leftrightarrow \mathbf{A}\mathbf{h}_a)}{\varepsilon' + \varepsilon b \mathbf{n}^T \mathbf{b}^\times \mathbf{J}^{-1} \mathbf{b}^\times \mathbf{n}} \tag{27}$$

Note that $\mathbf{J}^{-1}\mathbf{m} = \boldsymbol{\omega}$. It is evident that these equations are in the form of singularly perturbed differential equations.

Perturbed Hamiltonian System

When $\varepsilon = 0$, these equations reduce to the equations for a rigid N-rotor gyrostat (of dimension $3 + N$), for which Eq. (21) is a noncanonical Hamiltonian system.[15] Therefore the equations of motion may be rewritten as a perturbation from the simple gyrostat equations as

$$\dot{\mathbf{h}} = \mathbf{h}^\times \nabla H_o + \varepsilon \mathbf{f}_1(\mathbf{h}, \mathbf{h}_a, p_n, x; \varepsilon) \tag{28}$$

$$\dot{\mathbf{h}}_a = \mathbf{g}_a \tag{29}$$

$$\varepsilon \dot{p}_n = \Leftrightarrow c_d p_n \Leftrightarrow \varepsilon k x + \varepsilon f_2(\mathbf{h}, \mathbf{h}_a, p_n, x; \varepsilon) \tag{30}$$

$$\varepsilon \dot{x} = p_n + \varepsilon f_3(\mathbf{h}, \mathbf{h}_a, p_n, x; \varepsilon) \tag{31}$$

where

$$H_o = \frac{1}{2}\mathbf{h}^T \hat{\mathbf{J}} \mathbf{h} \Leftrightarrow \mathbf{h}_a^T \mathbf{A}^T \mathbf{J}_o^{-1} \mathbf{h} \tag{32}$$

$$\hat{\mathbf{J}} = \text{diag}\,(0, i_2, i_3) \tag{33}$$

and the inertia parameters i_2 and i_3 are defined as

$$i_2 = (J_1 \Leftrightarrow J_2)/(J_1 J_2), \quad i_3 = (J_1 \Leftrightarrow J_3)/(J_1 J_3) \tag{34}$$

and $\mathbf{J}_o = \mathbf{J}||_{\varepsilon=0}$. The $\varepsilon = 0$ version of these equations has been investigated in Refs. 13 and 14.

Remark on Numerical Results

All of the simulations illustrated in this paper were performed using MatLab[16] and Shampine and Reichelt's integration subroutines.[17] Two "tests" were used to verify accuracy of the numerical integrations. First, we checked to see that the angular momentum magnitude remained constant. Second, we integrated the differential equation for the total energy, and compared the result with the computed time history of the total energy. In both cases, the errors were consistent with the numerical accuracy properties of the integration subroutine used (ode45).

Equilibrium Motions

There are several possible equilibrium motions for the system described by Eqs. (21–24). In this paper we restrict our attention to those equilibria for which the damper is motionless; *i.e.*, $x = 0$ and $p_n = 0$. For these variables to remain zero, Eq. (24) also implies $y = 0$. Thus from the definition of y, one of the following conditions must hold:

$$\mathbf{J}^{-1}(\mathbf{h} \Leftrightarrow \mathbf{A}\mathbf{h}_a) \quad || \quad \mathbf{b} \tag{35}$$

$$\mathbf{b}^{\times}\mathbf{J}^{-1}(\mathbf{h} \Leftrightarrow \mathbf{A}\mathbf{h}_a) \quad \perp \quad \mathbf{n} \tag{36}$$

That is, either the angular velocity is parallel to the $\mathbf{b}$ axis, or the angular velocity is in the plane spanned by $\mathbf{b}$ and $\mathbf{n}$ (assuming that $\mathbf{b}$ and $\mathbf{n}$ are not parallel).

In addition, Eq. (21) implies that, for equilibrium, one of the following conditions must hold:

$$\mathbf{m} = \mathbf{0} \tag{37}$$

$$\mathbf{J}^{-1}\mathbf{m} \;||\; \mathbf{h} \tag{38}$$

With $y = 0$, the latter condition is equivalent to $\boldsymbol{\omega}||\mathbf{h}$, which is the usual condition used in determining rigid body equilibria, and has been used elsewhere to compute equilibria for gyrostats (*cf.* Hughes[1]). The former condition, $\mathbf{m} = \mathbf{J}_o\boldsymbol{\omega} = \mathbf{0}$, is of particular interest, because it is precisely the condition of a stationary platform, where all the angular momentum is in the rotors. Below, we will use this condition to investigate momentum transfer maneuvers which remain near this set of equilibria.

In the following section, we discuss some basic momentum transfer ideas for gyrostats without dampers. This is followed by a detailed treatment of an axial gyrostat with a damper aligned with the rotor axis.

Momentum Transfer for Gyrostats

Here we recall some results on momentum transfer in gyrostats (Refs. 8, 15, and 12). We assume that the control torques $\mathbf{g}_a$ are small, and may be expressed as $\mathbf{g}_a = \epsilon\boldsymbol{\sigma}$, where $|\epsilon| \ll 1$, and the elements of $\boldsymbol{\sigma}$ are $\mathcal{O}(1)$ or smaller. With the additional assumption that the elements of $\boldsymbol{\sigma}$ are constant, the method of averaging allows the approximate reduction of the $N + 3$ equations of motion [Eqs. (28–29), with $\varepsilon = 0$] to a single first-order differential equation for the slow evolution of the Hamiltonian. Furthermore, the $\mathbf{g}_a = \mathbf{0}$ branches of stable equilibria in the two-dimensional space spanned by H and the slow time $\tau = \epsilon t$ are integral curves of this averaged equation. The implication of these results is that constant-torque momentum transfer maneuvers which begin near a stable $\mathbf{g}_a = \mathbf{0}$ equilibrium will remain near the corresponding branch of stable equilibria until the stability properties of that branch change (*i.e.*, until a bifurcation occurs).

For $N \leq 2$, it is possible to interpret trajectories visually in the slow state space spanned by H and $\mathbf{h}_a$. In the following sections, we illustrate this by showing how to interpret the instability that can occur during maneuvers of single-rotor gyrostats with discrete dampers. We also demonstrate the so-called stationary-platform maneuver for gyrostats with $N \geq 2$.

Axial Gyrostat with Aligned Damper

We consider the relatively simple case of a single-rotor, axial gyrostat with $N = 1$, with rotor axis $\mathbf{a} = \mathbf{b}_1$. To further simplify the problem, we align the damper parallel to the rotor spin axis ($\mathbf{n} = \mathbf{b}_1$), and align the vector $\mathbf{b}$ with the $\mathbf{b}_3$ axis. (See Fig. 2.) The simplification of the equations of motion is evident and is not repeated here (*cf.* Hughes,[1] pp. 218–223).

For the calculations, the following parameters are used: $\mathbf{I} = \text{diag}(1.1, 0.8, 0.5), I_s = 0.1, \varepsilon = 0.3, c_d = 1$. Note that we have chosen $I_c^* = I_1^* \Leftrightarrow I_s^*$ so that $I_1' = I_1 \Leftrightarrow I_s = 1$. For these parameters, $i_2 = 0.25$ and $i_3 = 1$. The parameters b and k are chosen later to illustrate the stability characteristics of various motions.

Unperturbed Bifurcation Diagram

For $\varepsilon = 0$, the momentum transfer dynamics of the axial gyrostat are well-established.[4–8] The slow state space appears as shown in Fig. 3, where solid curves denote stable branches of equilibria and dashed curves denote unstable branches. The symbols $\mathbf{O}$, $\mathbf{P}$, $\mathbf{T}$, and $\mathbf{U}$ in the figure denote oblate, prolate, transverse, and unstable, according to which type of equilibrium the respective motions are (*cf.* Ref. 8). The oblate branch corresponds to a positive momentum about the $\mathbf{b}_1$ axis [$\mathbf{h} = (1, 0, 0)$], whereas the prolate branch corresponds to a negative momentum about the $\mathbf{b}_1$ axis [$\mathbf{h} = (\Leftrightarrow 1, 0, 0)$]. The transverse and unstable branches correspond roughly to spin about the $\mathbf{b}_2$ and $\mathbf{b}_3$ axes, but unless $h_a = 0$, these are not pure spins about these axes; rather there is a non-zero h_1 component. The bifurcations where $\mathbf{T}$ and $\mathbf{U}$ meet $\mathbf{P}$ are pitchforks, and occur when $h_a = i_3$ and i_2, respectively.

Perturbed Bifurcation Diagram

When $\varepsilon \neq 0$, the $\mathbf{U}$ branch is changed, and does not correspond to a branch of equilibria with $x = 0 = p_n$, since any angular velocity about the $\mathbf{b}_2$ axis induces a deflection in the damper mass [*cf.* Eq. (36)]. Since we are only interested in the equilibria for which $x = 0 = p_n$, we do not compute the new $\mathbf{U}$ branch here. The $\mathbf{T}$ branch is also changed, per Eq. (35), and for $h_a \neq 0$ does not satisfy the $x = 0 = p_n$ requirement, so we do not compute the new $\mathbf{T}$ branch.

The $\mathbf{O}$ and $\mathbf{P}$ branches hold the most interest here. That is, even though there are several relative equilibria for this system, the most useful equilibria are the steady spins about the $\mathbf{b}_1$ axis, defined by $(\mathbf{h}, h_a, p_n, x)_e = (\pm 1, 0, 0, h_a, 0, 0)$. The stability of these steady motions is of interest, and clearly depends on the value of h_a as well as the system parameters. From the symmetry of the problem (as evident in Fig. 3), we need only consider the $h_{1e} = +1$ case.[18] We develop the linearized stability conditions using the Routh-Hurwitz criteria (Ref. 1, Ch. 7 and App. A), which can be simplified to

$$I_1' > \Leftrightarrow \max(I_2, I_3)\lambda \tag{39}$$

$$k > \Leftrightarrow (\varepsilon^2 b \lambda^3)/(I_1'^2(I_1' + I_3\lambda)) \tag{40}$$

where $\lambda = h_a \Leftrightarrow 1$. The bifurcation diagram based on the first criterion is shown in Fig. 4; note that this does not take into account the spring stiffness. In the figure, the dashed lines denote unstable equilibria, the solid lines denote asymptotically stable equilibria, and the dot-dashed lines denote equilibria whose stability characteristics are determined by Eq. (40). The first of the two bifurcation points along the $\mathbf{P}$ branch persists (marked with $\times$), but past the first bifurcation (for $h_a > 0$), the $\mathbf{P}$ branch is unstable. By symmetry the $\mathbf{O}$ branch is unstable past the first bifurcation for $h_a < 0$.

Some specific cases are of interest. When $\lambda = \Leftrightarrow 1$ ($h_a = 0$), it is straightforward to show that

these are the familiar criteria for the spinning rigid body with a damper parallel to the spin axis.[3] When $\lambda = 0$, *i.e.*, when all of the angular momentum is in the rotor, then stability is guaranteed, since all of the stability conditions are met. When $\lambda > 0$, stability is also guaranteed.

When the first condition is not met, the equilibrium is unstable and no choice of damper parameters can stabilize the motion. This means that there is a critical value of $\lambda < 0$, denoted $\lambda^* = \Leftrightarrow I_1'/\max(I_2, I_3)$, that should not be within the operating range of the satellite. (Another way to put this is that $h_a > \Leftrightarrow \min(i_2, i_3)$ must be satisfied.) As a design consideration, then, it is appropriate to take

$$k > \Leftrightarrow (\varepsilon^2 b \lambda^{*3})/[I_1'^2(I_1' + I_3\lambda^*)] \tag{41}$$

With Eq. (41) satisfied, the entirety of the conditionally stable (dot-dashed) branches in Fig. 4 are asymptotically stable (assuming Eq. (41) is satisfied).

We should point out that the linear stability analysis is slightly complicated by the presence of a zero eigenvalue of the linearized system of equations. In fact, the first row and column of the linearized matrix are both zero. Thus the question of stability of the center manifold[19] must be addressed. In this problem, there is a first integral due to conservation of angular momentum, $h^2 = 1$. At the $\mathbf{O}$ and $\mathbf{P}$ equilibria, the value of this first integral is $h_1^2 = 1$. Since h_2, h_3, p_n, and x all approach 0 asymptotically (they are in the stable manifold), h_1 must approach ± 1 asymptotically to preserve the integral. If the initial conditions are sufficiently near the equilibrium, then h_1 must approach $+1$. Thus linear asymptotic stability implies nonlinear asymptotic stability. Of course, the equilibria are not necessarily globally stable. In particular, for small values of h_a, both the $\mathbf{O}$ and $\mathbf{P}$ branches are asymptotically stable. This is similar to the two asymptotically stable steady spins of a "quasi-rigid" body in different senses about the major axis.

Stable Momentum Transfer

In Figs. 5–7, we use the $h_a H$ plane to illustrate two stable momentum transfer maneuvers. In both maneuvers, the parameters $b = 1$ and $k = 0.36$ are chosen, satisfying Eq. (41). In the first maneu-

ver, the initial conditions (starting at $\times$ in the $h_a H$ plane) are $\mathbf{h} = (0.9206, 0.2762, 0.2762), h_a = 1, p_n = 0, x = 0$, and the torque is $g_a = \Leftrightarrow 0.05$. The maneuver time is 20 seconds (dimensionless), so that the rotor momentum goes from $h_a = 1$ to $h_a = 0$. Note that the trajectory moves from right to left in the figure, since $\dot{h}_a < 0$. This maneuver corresponds to despinning the rotor and spinning up the platform.

In the second maneuver, the initial conditions (starting at $\circ$ in the $h_a H$ plane) are $\mathbf{h} = (0.9206, 0.2762, 0.2762), 0, p_n = 0, x = 0$, and the torque is $g_a = 0.05$. Again the maneuver time is 20 seconds. This maneuver corresponds to spinning up the rotor and despinning the platform.

Both maneuvers are inherently stable, and as shown in Figs. 6 and 7, the states do asymptotically approach the equilibrium. In the first trajectory, continued momentum transfer would eventually reach the instability associated with $\lambda < \lambda^*$ and the corresponding pitchfork bifurcation. In the second trajectory, continued momentum transfer would increase λ and the trajectory would remain stable, asymptotically approaching the equilibrium state. In either case, continued numerical integration of the trajectory with $g_a = 0$ leads to asymptotic stability of the corresponding equilibrium point on the **O** branch.

Unstable Momentum Transfer

As noted above, there are at least two ways that an instability can occur. One is that k can be less than the critical value defined by Eq. (41), in which case an instability occurs when $\lambda = h_a \Leftrightarrow 1$ becomes less than the value defined by Eq. (40). The other is when a momentum transfer maneuver is attempted that passes through the critical value of λ^*. In Figs. 8–10, we illustrate two different unstable momentum transfer maneuvers. The first trajectory corresponds to identical initial conditions and system parameters as the first trajectory in Figs. 5–7 (starting at $\times$). The only difference is that here the momentum transfer is allowed to continue for 40 seconds, so that λ passes through λ^*, illustrating the fundamental instability that the spring stiffness cannot stabilize.

The second trajectory uses the same initial conditions as the second trajectory in Figs. 5–

7 (starting at $\circ$), but the stiffness, k, is taken to be less than the value required for stability at $h_a = 0 (\lambda = \Leftrightarrow 1)$. The specific value of k chosen is $k = 0.015 = \Leftrightarrow (\varepsilon^2 b \lambda^3)/[I_1'^2 (I_1' + I_3 \lambda)]$, with $\lambda = \Leftrightarrow 1/2$, so that once $h_a > 1/2$, the nominal equilibrium is stable. Also, for illustration, we use a smaller internal torque, $g_a = 0.01$, so that the instability has time to grow before the rotor stabilizes the motion. The momentum transfer time is 100 seconds. The figures illustrate the initial divergence of the trajectory, followed by an asymptotic approach to the equilibrium branch (*cf.* Fig. 5). Note especially the large departure of the the damper mass in Fig. 10, and how the growth in x reverses at $t \approx 50$ as expected ($t = 50 \Leftrightarrow h_a = 0.5$).

These examples serve to illustrate the effect of the damping mechanism on the success of certain spinup maneuvers for the axial gyrostat. In addition, the internal torque could be thought of as responding to the influence of external torques, as in the use of reaction wheels. From the definition of k in Eq. (10), it is evident that an increase of the angular momentum has the effect of decreasing the dimensionless stiffness. Thus, the limits imposed by the stability criteria in Eqs. (39–40) could also be used to determine the requirement for momentum unloading operations.

"Stationary-Platform" Maneuver

In this section we develop the concept of "stationary-platform" maneuvers for multi-rotor gyrostats. This class of maneuvers was previously reported for two-rotor gyrostats in Ref. 13. For two-rotor gyrostats, only a limited set of orientation changes is possible since the momentum of the rotors is confined to a plane. For three-rotor gyrostats, however, any orientation change is possible, provided that the wheels' saturation speeds are sufficiently large and that the wheels are not coplanar. The issue of saturation speeds was investigated in Ref. 20.

In the previous section, we showed that the stationary-platform equilibrium is asymptotically stable for all physically realizable system parameters, for the special case of the axial gyrostat with aligned damper [Eq. (40) with $\lambda = 0$]. Such explicit criteria are not readily available for the more general case of a multi-rotor gyrostat with arbitrarily aligned damper, but numerical

evidence based on a wide variety of system parameters suggests that this is so. In Ref. 14, we proved nonlinear stability for stationary-platform equilibria in the undamped case. In the present work, we numerically verify that the stationary-platform equilibria are asymptotically stable by computing the eigenvalues of the linearized system.

Referring to the earlier section on Momentum Transfer for Gyrostats, we consider the case when the elements of the internal torque vector, $\boldsymbol{\sigma}$, are not constant, but are slowly varying. It is reasonable to suppose that the results obtained for $\boldsymbol{\sigma}$ = constant still hold, and in fact they do. The stationary-platform maneuvers are based on these ideas applied to the special class of stationary-platform equilibria ($\mathbf{h} = \mathbf{A}\mathbf{h}_a$). The initial condition is near a stationary-platform equilibrium and the torques are chosen such that the rotor momenta satisfy the stationary-platform condition throughout the maneuver. Then, since the stationary-platform equilibria are all stable, the trajectories should remain near the branch of stationary-platform equilibria, and hence $\boldsymbol{\omega}$ should remain small. The advantage of such a trajectory is that the small platform angular velocities are less likely to excite vibrations in flexible components.

For stationary-platform maneuvers, we assume initial conditions on $\mathbf{h}$ and $\mathbf{h}_a$ such that $\mathbf{h} = \mathbf{A}\mathbf{h}_a$ and

$$\mathbf{h}_a^T \mathbf{A}^T \mathbf{A} \mathbf{h}_a = 1 \tag{42}$$

The latter condition defines an ellipsoid in the N-dimensional $\mathbf{h}_a$ space. The initial and desired final stationary-platform equilibria define two points on this ellipsoid. The spinup torques $\mathbf{g}_a$ are chosen such that the condition on $\mathbf{h}_a$ is satisfied throughout the maneuver. Differentiation of Eq. (42) with respect to time shows that any $\mathbf{g}_a$ which is orthogonal to $\mathbf{A}^T \mathbf{A} \mathbf{h}_a$ will yield such a maneuver. Thus the torque vector $\mathbf{g}_a = \epsilon \boldsymbol{\sigma}$ must lie in the tangent space of the ellipsoid. For the $N = 2$ case, the ellipsoid is a simple ellipse, and the trajectory in $\mathbf{h}_a$ space simply traces the ellipse. For the $N = 3$ case, there are infinitely many choices for the trajectory, since there are infinitely many curves connecting any two points on the ellipsoid.

One choice would be to take a geodesic which connects the two points, but this leads to complicated calculations and usually the ellipsoid will be nearly spherical. Therefore we choose to take a path which lies in the intersection of the ellipsoid with a plane passing through the origin and containing the initial and final values of $\mathbf{h}_a$, denoted $\mathbf{h}_{ao}$ and $\mathbf{h}_{af}$, respectively.

The development proceeds as follows. Define a new reference frame in $\mathbf{h}_a$ space with base vectors

$$\mathbf{c}_1 = \mathbf{h}_{ao}/\|\mathbf{h}_{ao}\| \tag{43}$$

$$\mathbf{c}_2 = \mathbf{c}_3^{\times}\mathbf{c}_1 \tag{44}$$

$$\mathbf{c}_3 = \mathbf{h}_{ao}^{\times}\mathbf{h}_{af}/\|\mathbf{h}_{ao}^{\times}\mathbf{h}_{af}\| \tag{45}$$

Collect these column matrices into a 3×3 rotation matrix:

$$\mathbf{C} = [\mathbf{c}_1 \;\; \mathbf{c}_2 \;\; \mathbf{c}_3] \tag{46}$$

Define a transformed rotor momentum vector $\boldsymbol{\nu}$ by

$$\boldsymbol{\nu} = \mathbf{C}^T\mathbf{h}_a \tag{47}$$

Under this transformation, the stationary-platform condition becomes

$$\boldsymbol{\nu}^T\mathbf{D}^T\mathbf{D}\boldsymbol{\nu} = 1 \tag{48}$$

where $\mathbf{D} = \mathbf{AC}$. The columns of $\mathbf{D}$, to be denoted $\mathbf{d}_j$, are not unit vectors, even though the columns of $\mathbf{A}$ are. Equation (48) defines the ellipsoid in terms of the components of $\boldsymbol{\nu}$, and it is

evident that $\boldsymbol{\nu}_o$ and $\boldsymbol{\nu}_f$ lie in the $\nu_1\nu_2$ plane. Thus $\nu_3 = 0$ for our chosen trajectory, and Eq. (48) simplifies to

$$\begin{bmatrix} \nu_1 & \nu_2 \end{bmatrix} \begin{bmatrix} d_1^2 & \mathbf{d}_1^T\mathbf{d}_2 \\ \mathbf{d}_1^T\mathbf{d}_2 & d_2^2 \end{bmatrix} \begin{bmatrix} \nu_1 \\ \nu_2 \end{bmatrix} = 1 \tag{49}$$

Now, for the trajectory to follow the ellipse defined by Eq. (49), it is sufficient to take

$$\begin{bmatrix} \dot{\nu}_1 \\ \dot{\nu}_2 \end{bmatrix} = \epsilon \begin{bmatrix} \Leftrightarrow\mathbf{d}_1^T\mathbf{d}_2 & \Leftrightarrow d_2^2 \\ d_1^2 & \mathbf{d}_1^T\mathbf{d}_2 \end{bmatrix} \begin{bmatrix} \nu_1 \\ \nu_2 \end{bmatrix} \tag{50}$$

or

$$\dot{\boldsymbol{\nu}} = \epsilon \begin{bmatrix} \Leftrightarrow\mathbf{d}_1^T\mathbf{d}_2 & \Leftrightarrow d_2^2 & 0 \\ d_1^2 & \mathbf{d}_1^T\mathbf{d}_2 & 0 \\ 0 & 0 & 0 \end{bmatrix} \boldsymbol{\nu} = \epsilon\mathbf{E}\boldsymbol{\nu} \tag{51}$$

It is evident that $\dot{\boldsymbol{\nu}}$ is orthogonal to $\mathbf{D}^T\mathbf{D}\boldsymbol{\nu}$, thus satisfying the conditions for a stationary-platform maneuver. Substituting $\boldsymbol{\nu} = \mathbf{C}^T\mathbf{h}_a$ into the control leads to the desired control law for the rotor torques:

$$\dot{\mathbf{h}_a} = \epsilon\mathbf{C}\mathbf{E}\mathbf{C}^T\mathbf{h}_a \tag{52}$$

This is a control law which yields a stationary-platform maneuver. Since $\mathbf{C}$ and $\mathbf{E}$ are constant matrices depending only on $\mathbf{A}$ and the initial and final values of $\mathbf{h}_a$, this is a constant coefficient linear system of equations. Since $\mathbf{h}_a$ lies on the ellipsoid, it is evident that the torques are bounded, and are $\mathcal{O}(\epsilon)$. Equation (52) can be solved in closed form and is decoupled from the platform dynamics. Thus the stationary-platform maneuver is an easy-to-implement open-loop maneuver which is nearly optimal in two ways: the platform angular velocity is small throughout the maneuver, and the motor torque is small throughout the maneuver, since $\|\mathbf{g}_a\| = \mathcal{O}(\epsilon)$. It is also possible

to view this control as a closed-loop control, since $\mathbf{h}_a$ may be expressed in terms of the relative angular velocities of the rotors (as might be measured by tachometers) and the platform angular velocities (as might be measured by accelerometers).

For an example, we use the same parameters as for axial gyrostat examples above, with two additional rotors aligned with the $\mathbf{b}_2$ and $\mathbf{b}_3$ axes. The initial conditions are $\mathbf{h} = (0.9206, 0.2762, 0.2762), \mathbf{h}_a = \mathbf{h}, p_n = 0, x = 0$, and the desired final conditions are $\mathbf{h} = (\Leftrightarrow 0.2762, \Leftrightarrow 0.9206, \Leftrightarrow 0.2762), \mathbf{h}_a = \mathbf{h}, p_n = 0, x = 0$. This corresponds to a maneuver through approximately 126°. Taking $\epsilon = 0.05$, the maneuver takes approximately 44 seconds. The angular momentum components and the particle momentum and position are shown in Fig. 11. The angular momentum reaches the desired final state, and the particle deflections are small.

For comparison, Fig. 12 shows the results of a constant torque maneuver from the initial to final values of rotor momentum. The torque magnitude is $\epsilon = 0.0293$, chosen so that the maneuver takes the same time as the stationary-platform maneuver. The trajectories in $\mathbf{h}$ space are similar, but the particle deflection is two orders of magnitude greater than in the stationary-platform case. In Fig. 13, we show a comparison of the magnitude of the angular velocity vectors for the two maneuvers, as well as the angle θ between the angular momentum vector and the desired angular momentum vector. For the constant torque maneuver, the angular velocity reaches ≈ 0.6 rad/s, whereas for the stationary-platform maneuver, the maximum angular velocity magnitude is ≈ 0.1 rad/s. Note that if a pure eigenaxis rotation is used for this maneuver, the angular velocity would be about 0.035 rad/s, and that the average value for the stationary-platform maneuver is about 0.051 rad/s. Thus the stationary-platform maneuver is a simple approximation to an eigenaxis maneuver.

Conclusions

The combination of a discrete damper and a set of flywheels has significant effects on the motion of an otherwise rigid satellite. The system of equations describing the motion of such a satellite model is a perturbation of a non-canonical Hamiltonian system, and the underlying Hamiltonian

structure is useful for understanding the dynamics. For the specific case of a single-rotor gyrostat with rotor and damper aligned with the major principal axis, it is possible to obtain explicit stability criteria that can be used in damper design, or in planning of momentum unloading operations. The Hamiltonian bifurcation diagram is an effective tool for interpretation of potential instabilities during attitude maneuvers. For multi-rotor gyrostats, explicit stability criteria are not available. Stationary-platform equilibria, however, appear to be asymptotically stable for all values of system parameters. This apparent fact leads to the usefulness of a class of attitude maneuvers based on steering the rotors along an ellipsoid defined by the stationary-platform condition. These stationary-platform maneuvers are significantly better than constant torque maneuvers in terms of angular velocity magnitude and the magnitude of excitation of the flexible component.

References

[1]Hughes, P. C., *Spacecraft Attitude Dynamics*, Wiley, New York, 1986.

[2]Chang, C. O., Liu, L. Z., and Alfriend, K. T., "Dynamics and Stability of a Freely Precessing Spacecraft Containing a Nutation Damper," *Journal of Guidance, Control and Dynamics*, Vol. 19, No. 2, 1996, pp. 297–305.

[3]Chinnery, A. E. and Hall, C. D., "Motion of a Rigid Body with an Attached Spring-Mass Damper," *Journal of Guidance, Control and Dynamics*, Vol. 18, No. 6, 1995, pp. 1404–1409.

[4]Barba, P. M. and Aubrun, J. N., "Satellite Attitude Acquisition by Momentum Transfer," *AIAA Journal*, Vol. 14, No. 10, 1976, pp. 1382–1386.

[5]Gebman, J. R. and Mingori, D. L., "Perturbation Solution for the Flat Spin Recovery of a Dual Spin Spacecraft," *AIAA Journal*, Vol. 14, No. 7, 1976, pp. 859–867.

[6]Junkins, J. L. and Turner, J. D., *Optimal Spacecraft Rotational Maneuvers*, Elsevier, Amsterdam, 1986.

[7]Hubert, C. H., "Spacecraft Attitude Acquisition from an Arbitrary Spinning or Tumbled State," *Journal of Guidance and Control*, Vol. 4, No. 2, 1981, pp. 164–170.

[8]Hall, C. D. and Rand, R. H., "Spinup Dynamics of Axial Dual-Spin Spacecraft," *Journal of Guidance, Control and Dynamics*, Vol. 17, No. 1, 1994, pp. 30–37.

[9]Mazzoleni, A. P., Hall, C. D., and Stabb, M. C., "Double Averaging Approach to the Study of Spinup Dynamics of Flexible Satellites," *Journal of Guidance, Control and Dynamics*, Vol. 19, No. 1, 1996, pp. 54–59.

[10]Anchev, A. A., "Equilibrium Attitude Transitions of a Three-Rotor Gyrostat in a Circular Orbit," *AIAA Journal*, Vol. 11, No. 4, 1973, pp. 467–472.

[11]Krishnan, H., McClamroch, N. H., and Reyhanoglu, M., "Attitude Stabilization of a Rigid Spacecraft Using Two Momentum Wheel Actuators," *Journal of Guidance, Control and Dynamics*, Vol. 18, No. 2, 1995, pp. 256–263.

[12]Hall, C. D., "Momentum Transfer in Torque-Free Gyrostats," In *Nonlinear Dynamics*, A. Guran (editor), World Scientific, Singapore, 1995.

[13]Hall, C. D., "Momentum Transfer in Two-Rotor Gyrostats," *Journal of Guidance, Control and Dynamics*, Vol. 19, No. 5, 1996, pp. 1157–1161.

[14]Hall, C. D., "Stationary-Platform Maneuvers of Gyrostat Satellites," In *Dynamics and Control of Structures in Space III*, C.L. Kirk and D. J. Inman (editors), Computational Mechanics Publications, Southampton, 1996, pp. 337–348.

[15]Hall, C. D., "Spinup Dynamics of Gyrostats," *Journal of Guidance, Control and Dynamics*, Vol. 18, No. 5, 1995, pp. 1177–1183.

[16]*MATLAB Reference Guide*, The MathWorks, Inc., Natick, MA, 1996.

[17]Shampine, L. F. and Reichelt, M. W. The MATLAB ODE Suite. Technical report, 1996.

[18]Hall, C. D., "Equivalence of Two Classes of Dual-Spin Spacecraft Spinup Problems," *Journal of Guidance, Control and Dynamics*, Vol. 15, No. 4, 1992, pp. 1032–1034.

[19]Carr, J., *Applications of Center Manifold Theory*, Springer-Verlag, New York, 1981.

[20]Schultz, G. W. Optimal Spacecraft Attitude Maneuvers Using Momentum Wheels. Master's thesis, Graduate School of Engineering, Air Force Institute of Technology, Wright-Patterson AFB, Ohio, 1995.

Figure Captions

Figure 1. N-Rotor gyrostat with discrete damper.

Figure 2. Single-rotor axial gyrostat with aligned discrete damper.

Figure 3. The $h_a H$ plane for an axial gyrostat.

Figure 4. The $h_a H$ plane for an axial gyrostat with damper.

Figure 5. Stable momentum transfer maneuvers in the $h_a H$ plane.

Figure 6. Angular momentum components for stable momentum transfer maneuvers.

Figure 7. Damper momentum and position for stable momentum transfer maneuvers.

Figure 8. Unstable momentum transfer in the $h_a H$ plane.

Figure 9. Angular momentum components for unstable momentum transfer maneuvers.

Figure 10. Damper momentum and position for unstable momentum transfer maneuvers.

Figure 11. Angular momentum and damper momentum and position for stationary-platform maneuver.

Figure 12. Angular momentum and damper momentum and position for constant-torque maneuver.

Figure 13. Angular velocity magnitude and "cone" angle for stationary-platform and constant-torque maneuvers.

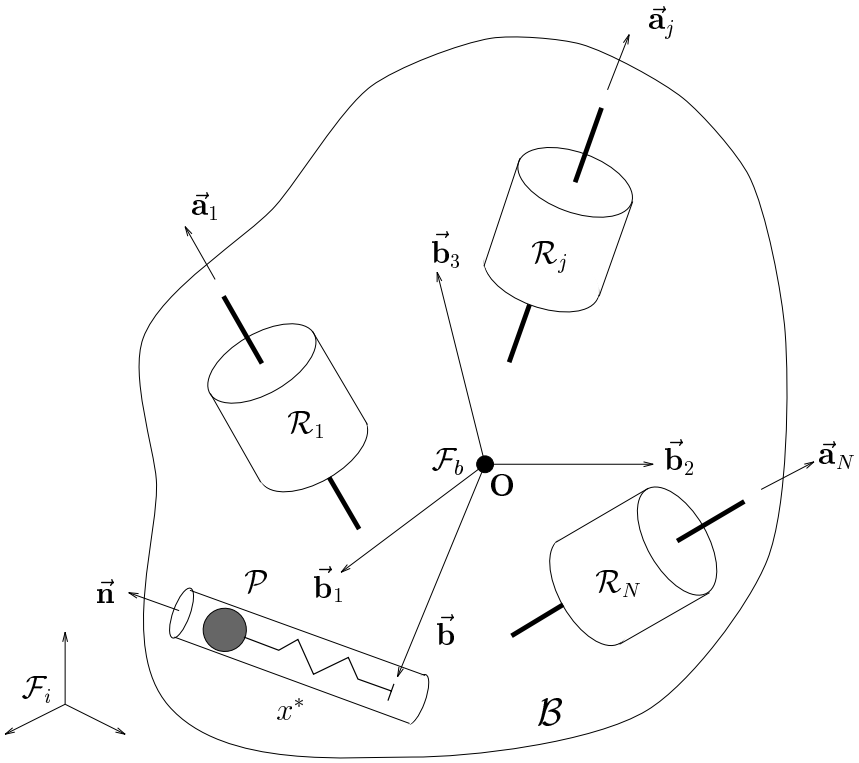
$\vec{\mathbf{a}}_j$
$\vec{\mathbf{a}}_1$
$\vec{\mathbf{b}}_3$
$\mathcal{R}_j$
$\mathcal{R}_1$
$\mathcal{F}_b$
$\mathbf{O}$
$\vec{\mathbf{b}}_2$
$\vec{\mathbf{a}}_N$
$\vec{\mathbf{n}}$
$\mathcal{P}$
$\vec{\mathbf{b}}_1$
$\mathcal{R}_N$
$\vec{\mathbf{b}}$
$\mathcal{F}_i$
x^*
$\mathcal{B}$

C. D. Hall

Fig. 1

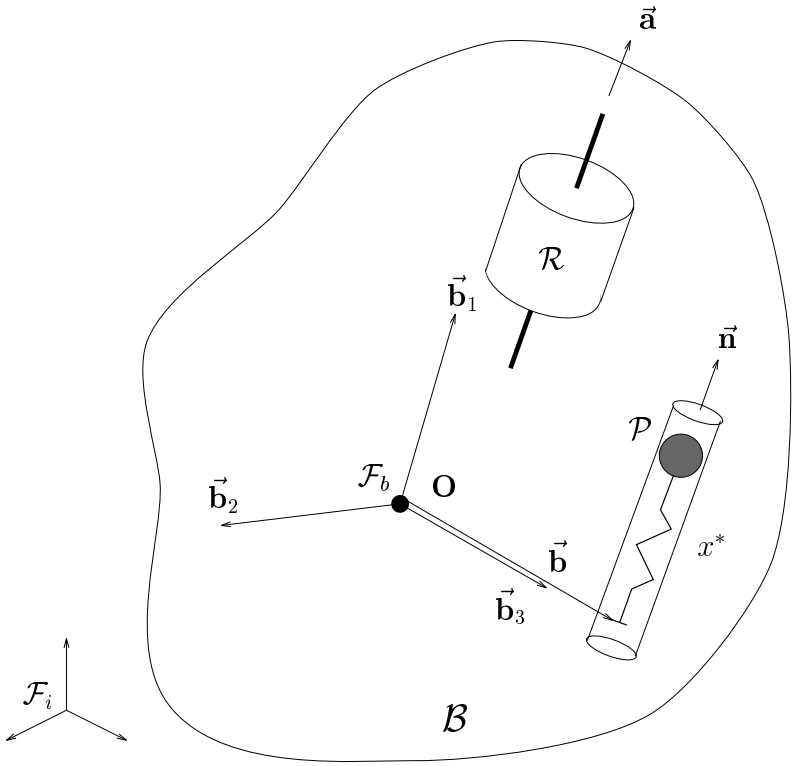
$\vec{\mathbf{a}}$
$\mathcal{R}$
$\vec{\mathbf{b}}_1$
$\vec{\mathbf{n}}$
$\mathcal{P}$
$\mathcal{F}_b$
$\mathbf{O}$
$\vec{\mathbf{b}}_2$
$\vec{\mathbf{b}}$
x^*
$\vec{\mathbf{b}}_3$
$\mathcal{F}_i$
$\mathcal{B}$

C. D. Hall

Fig. 2

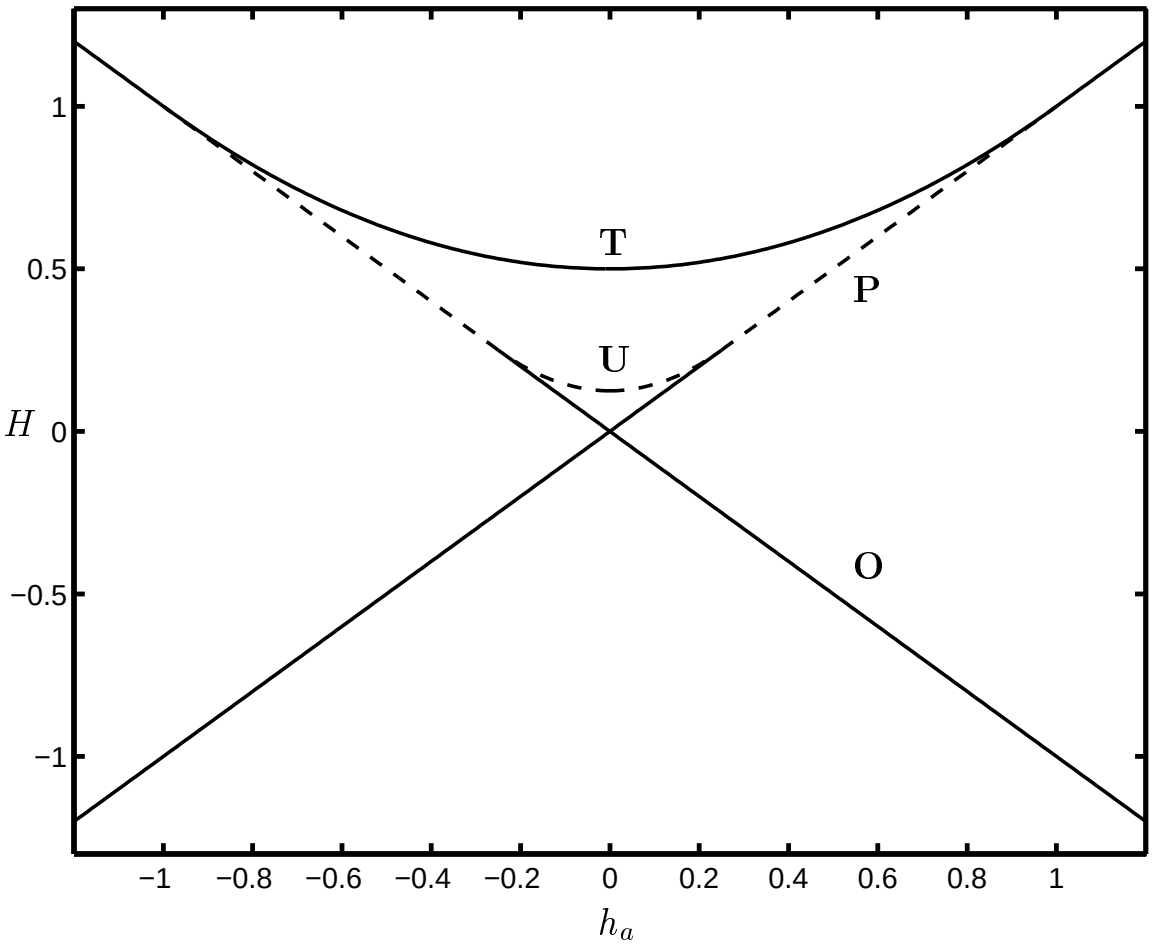

C. D. Hall

Fig. 3

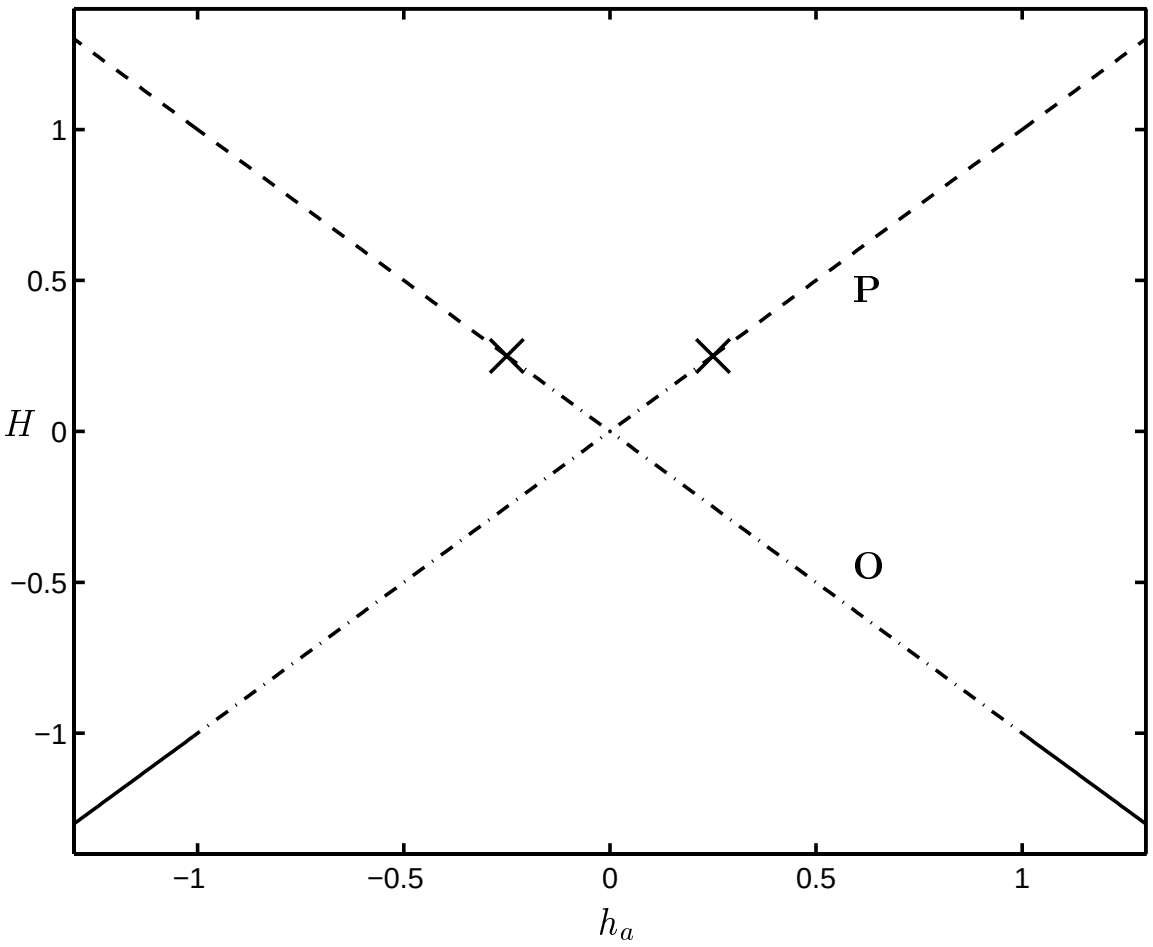

C. D. Hall

Fig. 4

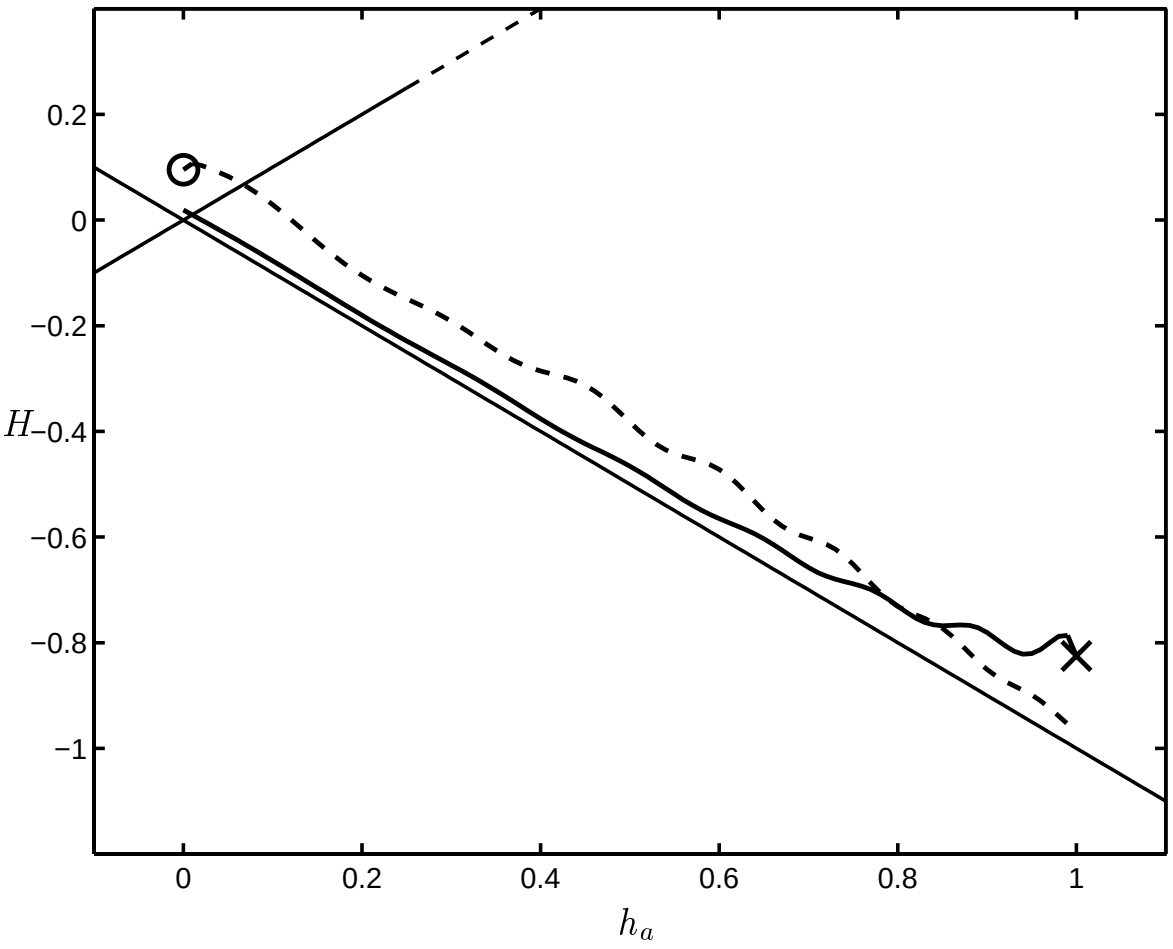

C. D. Hall

Fig. 5

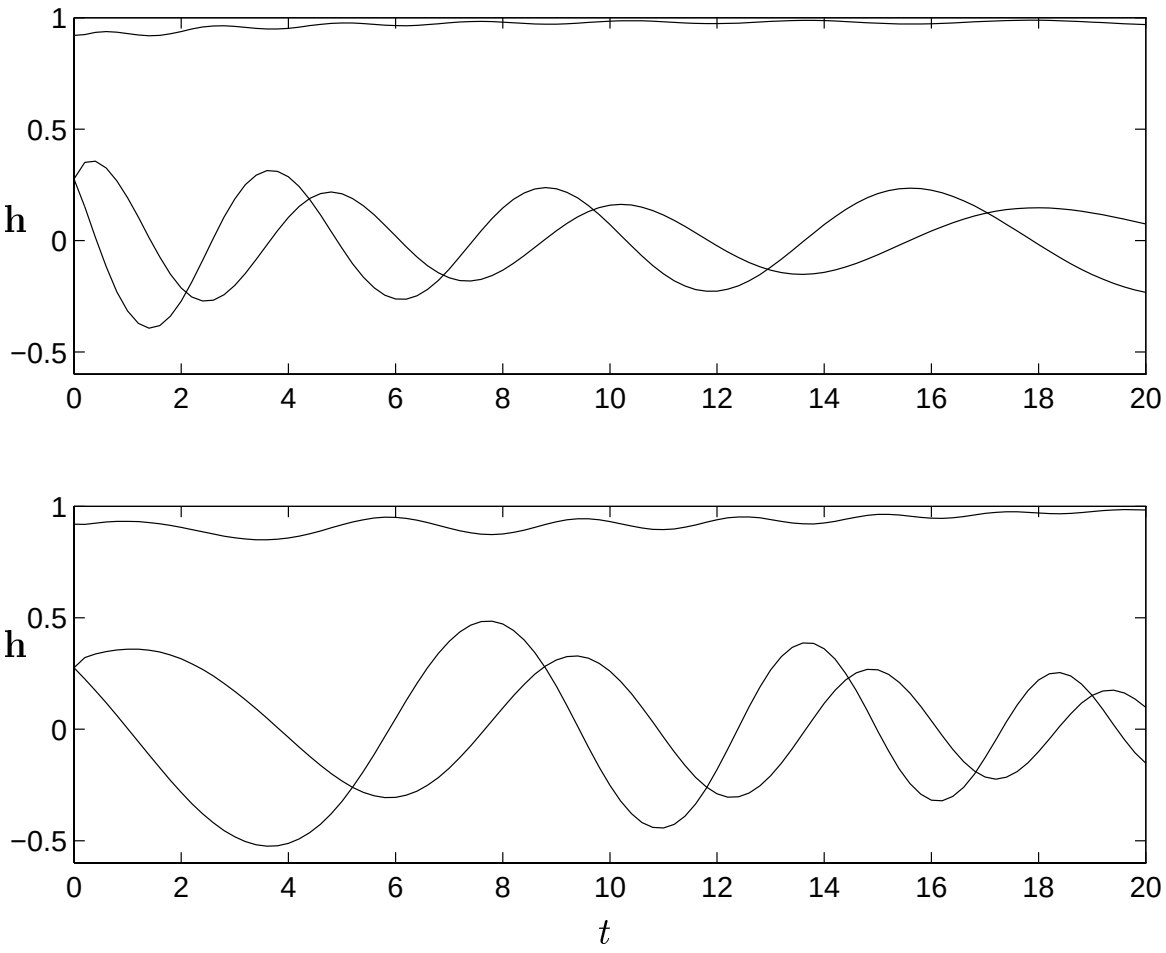

C. D. Hall

Fig. 6

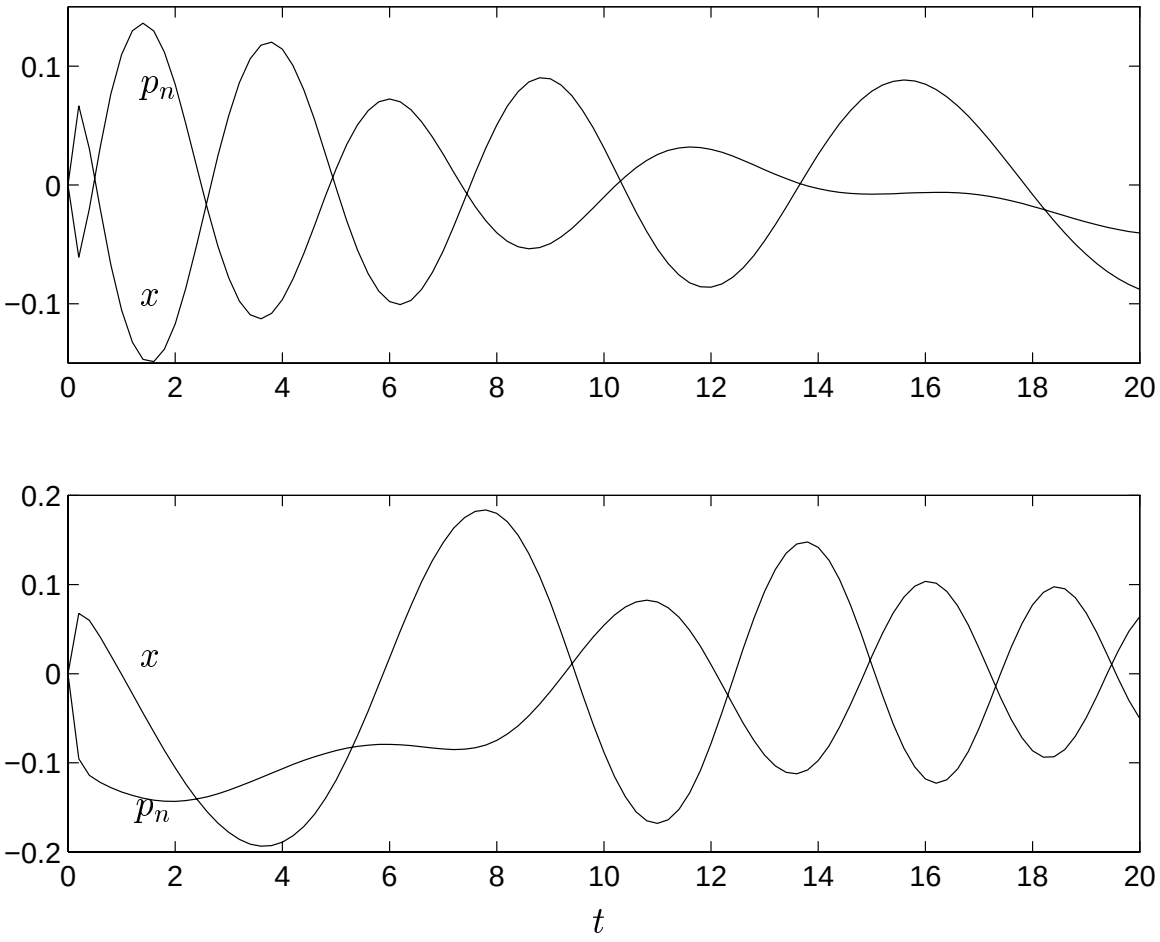

C. D. Hall

Fig. 7

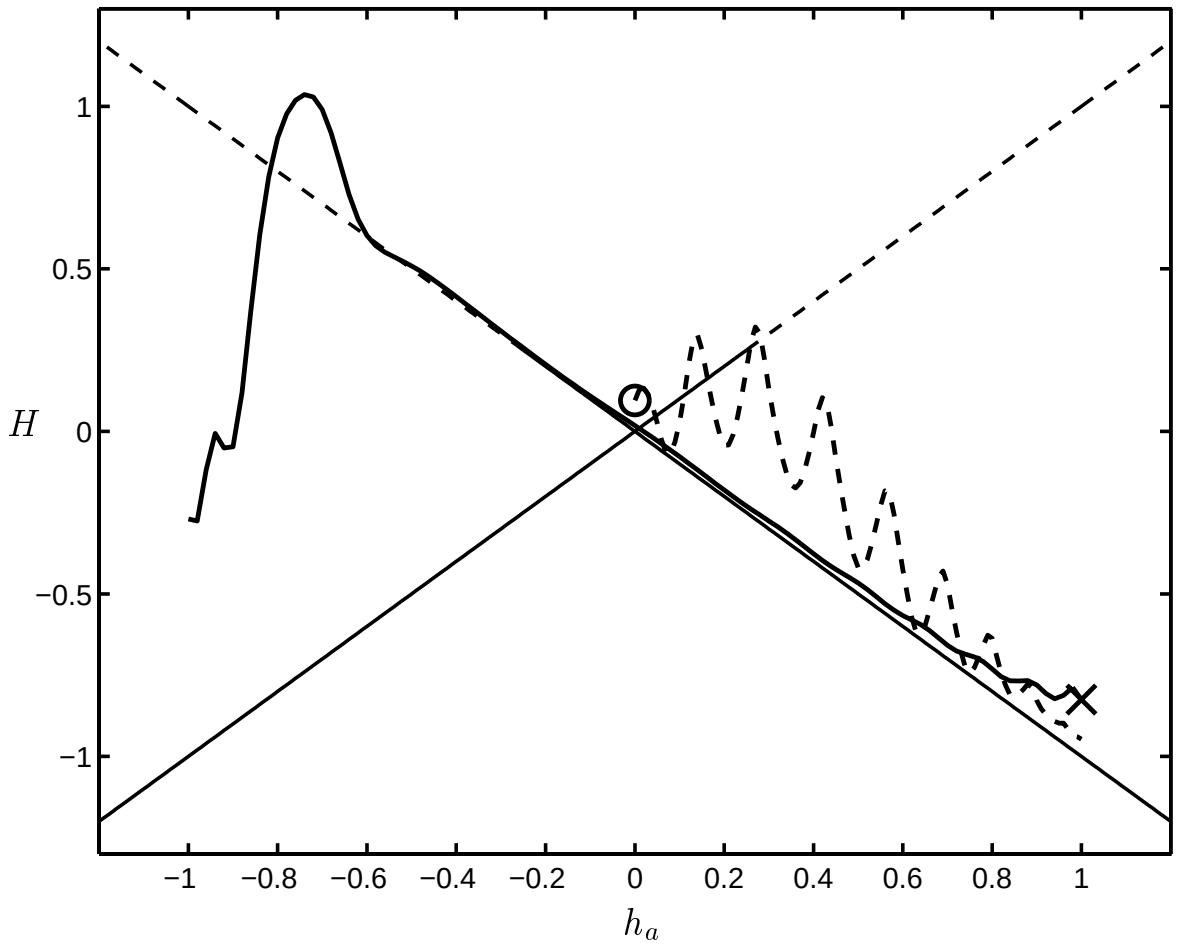

C. D. Hall

Fig. 8

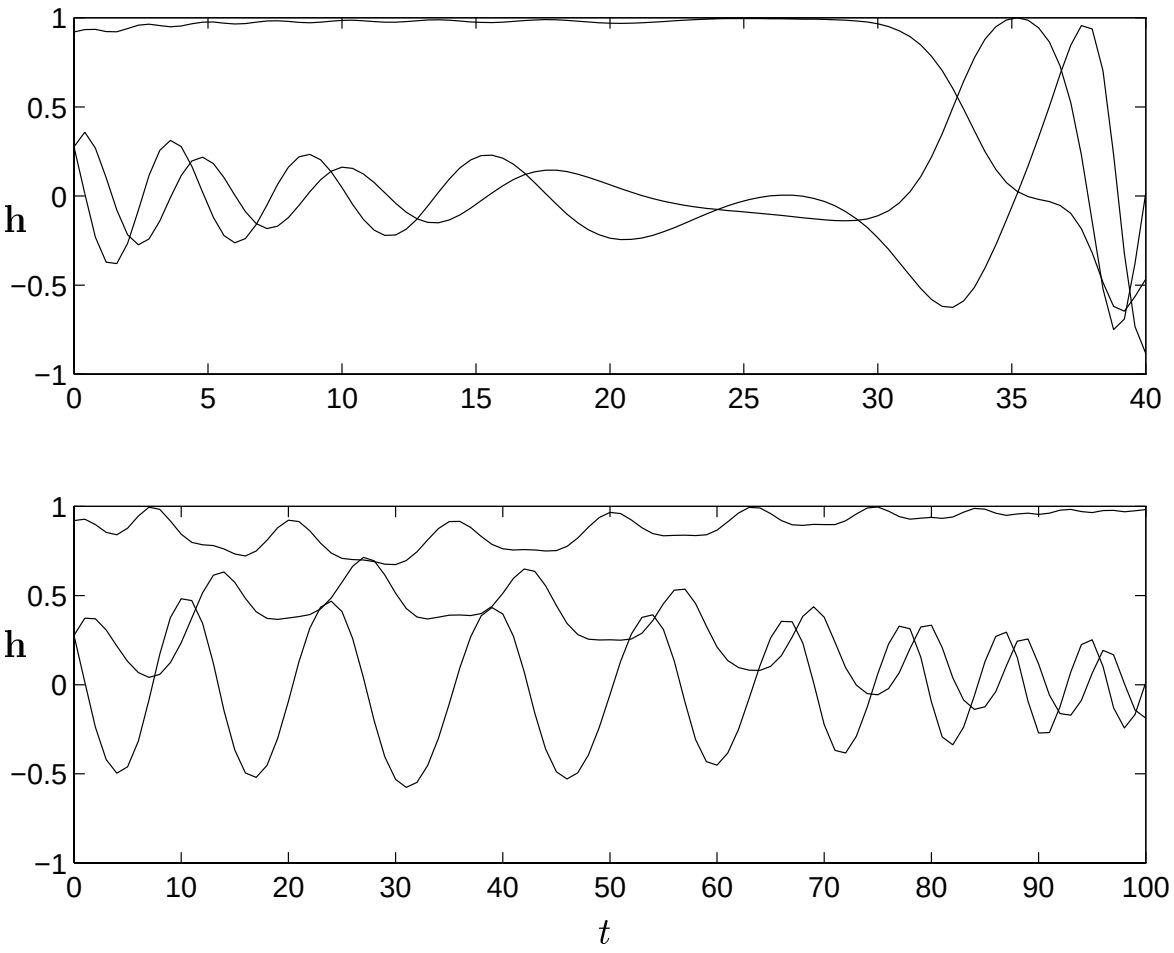
h
1
0.5
0
−0.5
−1
0
5
10
15
20
25
30
35
40
h
1
0.5
0
−0.5
−1
0
10
20
30
40
50
60
70
80
90
100
t

C. D. Hall

Fig. 9

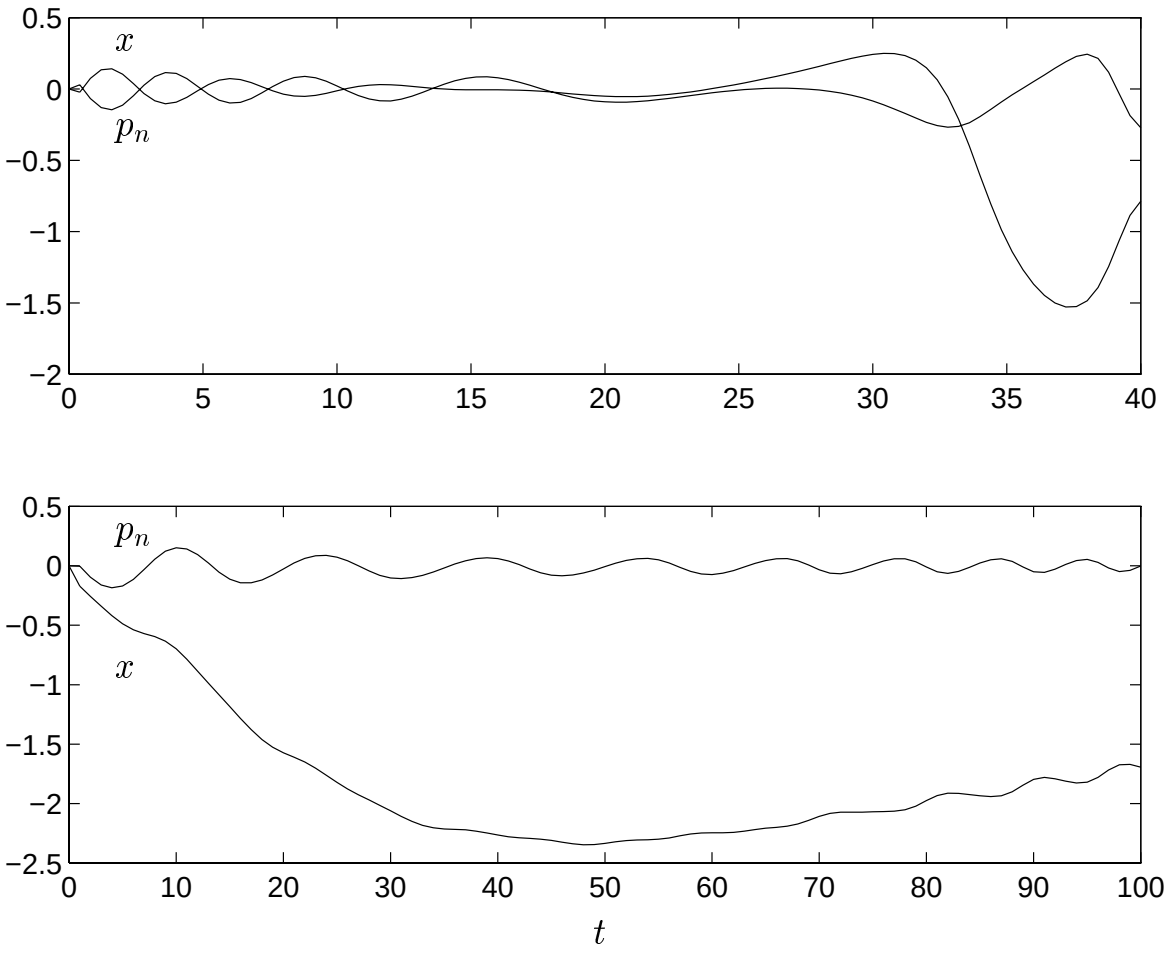

C. D. Hall

Fig. 10

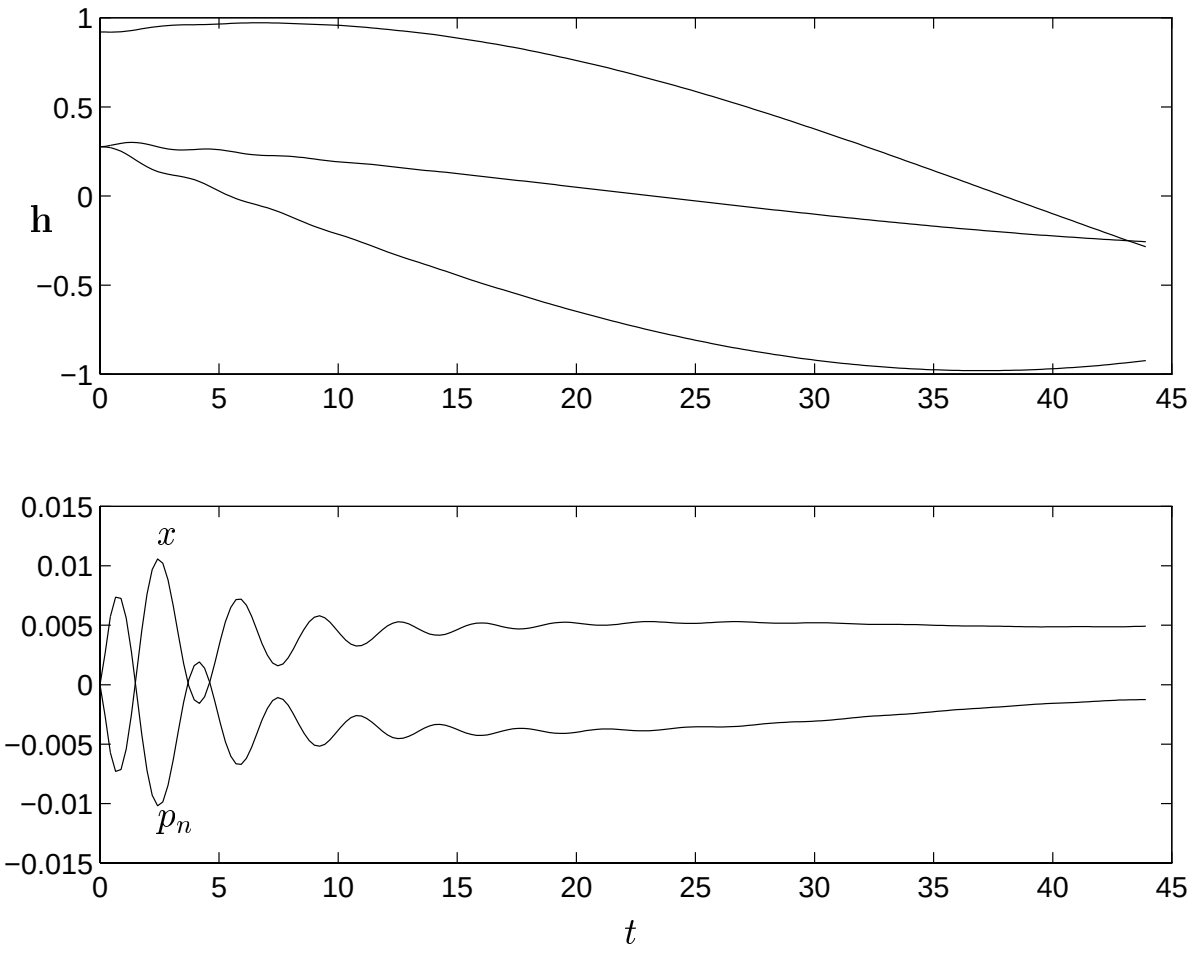

C. D. Hall

Fig. 11

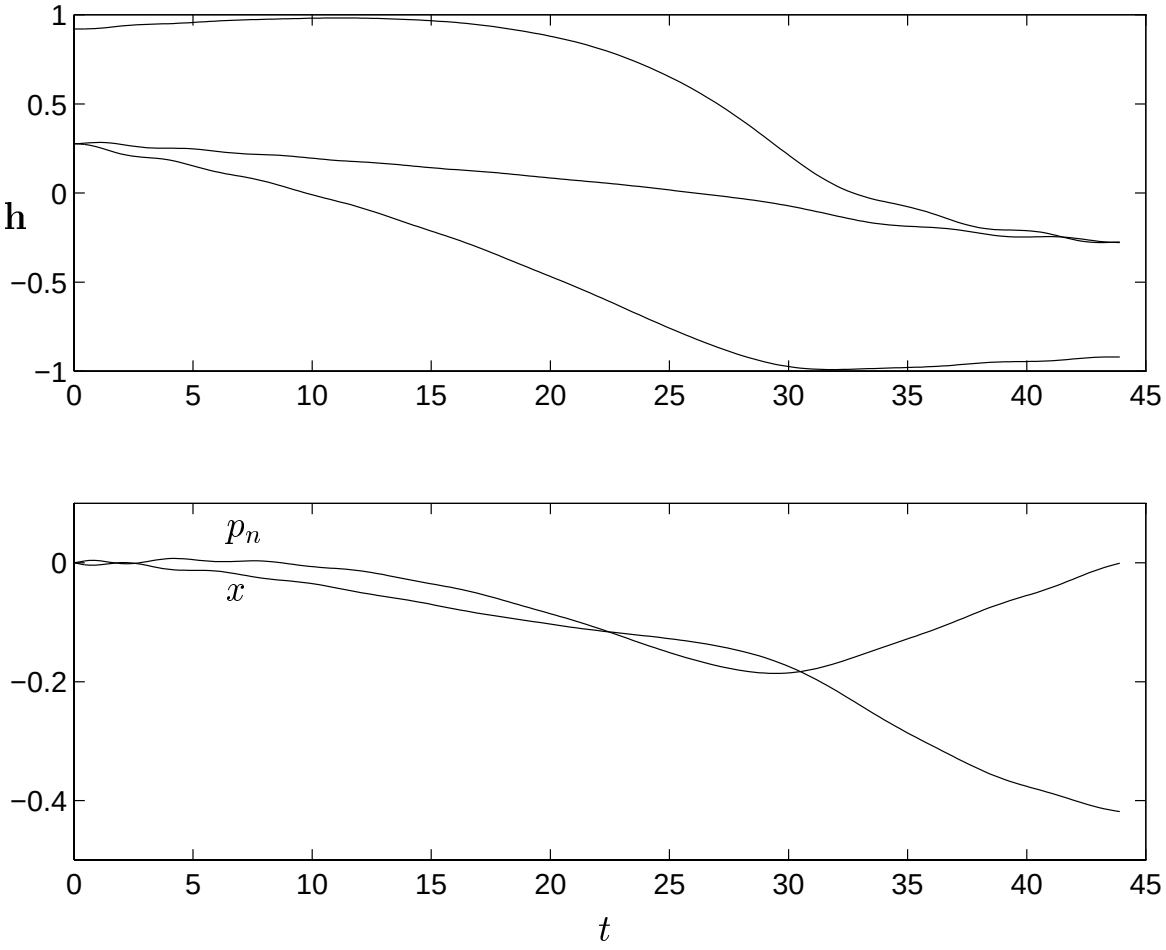

C. D. Hall

Fig. 12

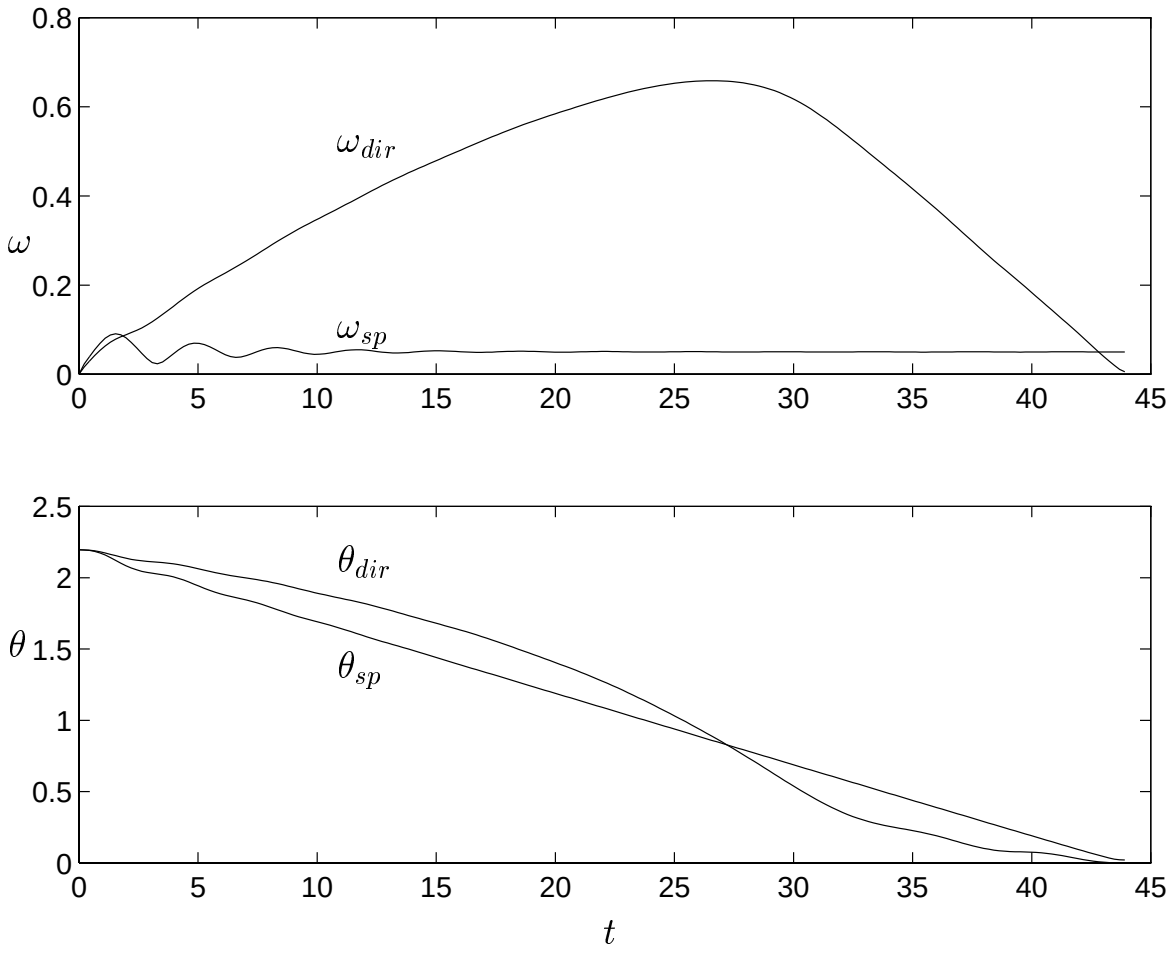

C. D. Hall

Fig. 13